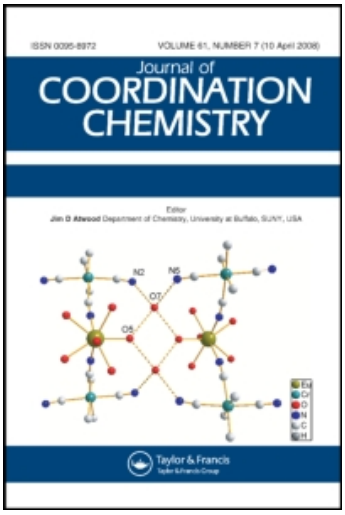

**Journal of Coordination Chemistry**
Publication details, including instructions for authors and subscription information:
http://www.informaworld.com/smpp/title~content=t713455674

# An organic-inorganic polymer with Keggin-type polyoxoanions as building blocks: preparation, characterization and crystal structure of $\{H[Ba(DMF)_6PMo_{12}O_{40}]\cdot(dma)\}_{<i>n</i>}$

Jingping Wang[a]; Jie Li[a]; Jingyang Niu[ab]
[a] Institute of Molecule and Crystal Engineering, School of Chemistry and Chemical Engineering Henan University, Kaifeng 475001, P.R. China [b] State Key Laboratory of Coordination Chemistry, Nanjing University, Nanjing 210093, P.R. China

**To cite this Article** Wang, Jingping , Li, Jie and Niu, Jingyang(2005) 'An organic-inorganic polymer with Keggin-type polyoxoanions as building blocks: preparation, characterization and crystal structure of $\{H[Ba(DMF)_6PMo_{12}O_{40}]\cdot(dma)\}_{<i>n</i>}$', Journal of Coordination Chemistry, 58: 18, 1639 — 1651
**To link to this Article: DOI:** 10.1080/00958970500148404
**URL:** http://dx.doi.org/10.1080/00958970500148404

*Journal of Coordination Chemistry*
Vol. 58, No. 18, December 2005, 1639–1651



# An organic–inorganic polymer with Keggin-type polyoxoanions as building blocks: preparation, characterization and crystal structure of $\{H[Ba(DMF)_6PMo_{12}O_{40}]\cdot(dma)\}_n$

JINGPING WANG†, JIE LI† and JINGYANG NIU*†‡

†Institute of Molecule and Crystal Engineering, School of Chemistry and Chemical Engineering Henan University, Kaifeng 475001, P.R. China
‡State Key Laboratory of Coordination Chemistry, Nanjing University, Nanjing 210093, P.R. China



(*Received 14 October 2004; revised 29 November 2004; in final form 18 April 2005*)

A novel organic–inorganic polymer of $\{H[Ba(DMF)_6(PMo_{12}O_{40})]\cdot(dma)\}_n$ (dma = dimethylamine, DMF = N,N-dimethylformamide) has been synthesized and characterized. Single-crystal X-ray structural analysis indicates that the title compound crystallizes in a monoclinic lattice, $C2/c$ with $a = 22.336(5)$, $b = 12.798(3)$, $c = 21.498(4)$ Å, $\beta = 99.77(3)^\circ$, $Z = 4$, $V = 6065(2)$ Å$^3$, $D_c = 2.673$ Mg m$^{-3}$, $F(000) = 4620$, $R_1 = 0.0600$, $wR_2 = 0.1125$. Crystal structural analysis reveals that $Ba^{2+}$ ion lies in a distorted square antiprismatic environment with eight oxygen atoms, six from DMF molecules and two from adjacent polyanions. $[Ba(DMF)_6]^{2+}$ ions coordinated to $[PMo_{12}O_{40}]^{3-}$ building blocks form a 1D corrugated chain. The results of the single crystal X-ray diffraction and IR spectra show the metal cations are coordinated to Keggin clusters. The ESR spectra show that the title compound is strongly photosensitive towards sunlight. Cyclic voltammetry shows that the title compound undergoes five two-electron reversible reductions and the $[PMo_{12}O_{40}]^{3-}$ anions are the active centers for electrochemical redox reactions in solution.

*Keywords:* Synthesis; Polyoxometalates; Crystal structure; Keggin structure

## 1. Introduction

Heteropoly compounds are a class of polynuclear coordination complexes, which have received increasing attention owing to their special structures, superior physical–chemical properties, applied prospects in catalysis, medicine, functional materials, photochemistry and potential applications of the organic–inorganic compounds formed by polyoxometalate electron acceptors and organic electron donors in optical, electrical, magnetic and superconductivity fields [1–8]. Crystal structures of many charge

*Corresponding author. Fax: +86-378-2853650. Tel.: +86-378-2192443. Email: jyniu@henu.edu.cn

*Journal of Coordination Chemistry*
ISSN 0095-8972 print: ISSN 1029-0389 online © 2005 Taylor & Francis
DOI: 10.1080/00958970500148404

transfer compounds were reported [9–12]. However, these compounds are unstable at room temperature. From the viewpoint of molecular design, we attempt to introduce metal ions coordinated to organic groups. One aim is to combine polyanions with organic groups through metal ions and make the organic–inorganic complexes stable, such that we can acquire information on the optical properties of these compounds. DMF molecules are electron-rich donors and can affect electron transfer. Finally, the combination of heavy atoms with high oxidation states and reduced polyoxometalate anions to form mixed-valence compounds can lead to crystals which exhibit photochromism. In this article, a complex $\{H[Ba(DMF)_6(PMo_{12}O_{40})] \cdot (dma)\}_n$ was prepared and characterized by elemental analysis and UV spectra. In its structure, the metal ions are coordinated by DMF and polyanion ligands to form a structure unit, and then these structure units are connected together through $Mo–O_d–Ba–O_d–Mo$ links to construct a one-dimensional chain-like structure. This article focuses primarily on solid-state structural aspects of organic–inorganic complexes and reveals the structure of the title compound in which infinite stacking assemblies between polyanions and cationic units are achieved.



## 2. Experimental

### 2.1. *Materials*

$\alpha$-$H_3PMo_{12}O_{40} \cdot nH_2O$ was prepared according to the literature [13] and confirmed by IR and UV spectra. All other chemicals used for synthesis were regent grade and used without further purification.

### 2.2. *Physical measurements and analyses*

IR spectra were recorded on a Nicolet 170 SXFT-IR spectrometer using KBr pellets in the 400–4000 $cm^{-1}$ range. UV spectra were obtained on a Shimazu UV-250 spectrophotometer between 190 and 400 nm (in water). C, H, N elemental analyses were performed on a Perkin-Elmer 240 C elemental analyzer. Thermogravimetric analysis (TG-DTA) was performed under air on a Perkin-Elmer-7 instrument with a heating rate of 10°C $min^{-1}$ from 20 to 700°C. Electrochemical measurements were performed on a LK98 microcomputer-based electrochemical system (LANLIKE, Tianjin, China). A three-electrode system was employed for cyclic voltammetry. A 4-mm diameter glass carbon disk electrode (GCE) (homemade) was used as a working electrode, a saturated calomel reference electrode (SCE) and a platinum wire served as the counter electrode. All electrochemical measurements were carried out at room temperature (25–30°C).

### 2.3. *Preparation of the title compound*

$BaCO_3$ (0.2 g, 1.1 mmol) and $\alpha$-$H_3PMo_{12}O_{40} \cdot nH_2O$ (2.0 g, 1.1 mmol) in the molar ratio of 1 : 1 were dissolved in 15 mL of water and heated at the temperature of 80°C until solids separated. The product was dissolved in 15 mL of acetonitrile and water in the ratio of 3 : 2 (v/v), and 1.0 mL DMF was added at room temperature with stirring. The resulting solution was refluxed at 80°C for 15 min and filtered off. The obtained

solution was left in the dark. Several days later, good yellow crystals suitable for X-ray diffraction were obtained. Anal. Calcd for $\{H[Ba(DMF)_6(PMo_{12}O_{40})]\cdot(dma)\}_n$ (%): C, 9.82; H, 2.04; N, 4.02. Found: C, 9.97; H, 1.98; N, 4.33.

### 2.4. *X-ray structure determination*

Crystal data collection parameters along with the final refinement are summarized in table 1. Selected bond lengths and bond angles are listed in tables 2 and 3, respectively.

A single crystal with dimension of $0.23 \times 0.18 \times 0.11\,mm^3$ was used for the data collection on a Rigaku RAXIS-IV image plate area detector with Mo K$\alpha$ ($\lambda = 0.71073$ Å) radiation at 293(2) K. The structure was solved by direct methods and refined by the full-matrix least-squares method on $F^2$ with SHELEXL 97 [14] to $R_1 = 0.0600$ ($wR_2 = 0.1125$) for 5164 independent reflections [$I > 2\sigma(I)$] collected in the range of $2.43 < \theta < 24.99^\circ$, $0 \le h \le 26$, $0 \le k \le 15$, $-25 \le l \le 15$. The intensity data were corrected for Lorentz and polarization effects as well as for empirical absorption [15]. The non-hydrogen atoms were refined anisotropically, and all hydrogen atoms



Table 1. Crystal data and structure refinement for the title compound.

| | |
|---|---|
| Formula | $C_{20}H_{50}BaMo_{12}N_7O_{46}P$ |
| Formula weight | 2444.20 |
| Crystal system | Monoclinic |
| Space group | *C*2/c |
| *a* (Å) | 22.336(5) |
| *b* (Å) | 12.798(3) |
| *c* (Å) | 21.498(4) |
| $\beta$ (°) | 99.77(3) |
| *V* (Å$^3$) | 6056(2) |
| *Z* | 4 |
| Reflections collected | 5164 |
| Independent reflections | 5164 |
| Final *R* induces [$I > 2\sigma(I)$] | $R_1 = 0.06000$, $wR_2 = 0.1125$ |
| Largest diff. peak and hole (e Å$^{-3}$) | 1.733 and −1.212 |

Table 2. Selected bond lengths (Å) of the title compound.

| | | | |
|---|---|---|---|
| Ba(1)–O(2A) | 2.664(10) | Ba(1)–O(3A) | 2.698(9) |
| Ba(1)–O(1A)#1 | 2.794(9) | Ba(1)–O(2) | 3.080(7) |
| P(1)–O(20′) | 1.491(12) | P(1)–O(19)#2 | 1.504(12) |
| P(1)–O(20)#2 | 1.549(12) | P(1)–O(19′) | 1.575(12) |
| Mo(1)–O(1) | 1.638(8) | Mo(1)–O(7) | 1.871(9) |
| Mo(1)–O(13) | 1.873(8) | Mo(1)–O(9)#2 | 1.928(8) |
| Mo(1)–O(15)#2 | 1.929(8) | Mo(1)–O(19′)#2 | 2.419(12) |
| Mo(2)–O(2) | 1.658(7) | Mo(2)–O(17) | 1.858(9) |
| Mo(2)–O(16) | 1.884(8) | Mo(2)–O(18) | 1.895(8) |
| Mo(2)–O(14) | 1.927(8) | Mo(2)–O(20) | 2.437(12) |
| Mo(3)–O(3) | 1.632(8) | Mo(3)–O(14) | 1.848(8) |
| Mo(3)–O(15) | 1.860(8) | Mo(3)–O(12) | 1.924(8) |
| Mo(3)–O(11)#2 | 1.945(8) | Mo(3)–O(19) | 2.438(12) |
| Mo(3)–O(20′) | 2.453(12) | Mo(4)–O(4) | 1.636(8) |
| Mo(4)–O(12) | 1.852(9) | Mo(4)–O(18) | 1.895(8) |
| Mo(4)–O(10) | 1.895(8) | Mo(4)–O(7) | 1.915(9) |
| Mo(4)–O(19′)#2 | 2.455(12) | Mo(4)–O(20′) | 2.496(12) |

Table 3. Selected bond angles (°).

| | | | |
|---|---|---|---|
| O(20′)–P(1)–O(20′)#2 | 180.0(8) | O(20′)–P(1)–O(19)#2 | 113.1(6) |
| O(20′)#2–P(1)–O(19)#2 | 66.9(6) | O(20′)–P(1)–O(19) | 66.9(6) |
| O(20′)#2–P(1)–O(19) | 113.1(6) | O(19)#2–P(1)–O(19) | 180.0(5) |
| O(20′)–P(1)–O(20)#2 | 110.0(6) | O(20′)#2–P(1)–O(20)#2 | 70.0(6) |
| O(19)#2–P(1)–O(20)#2 | 109.1(7) | O(19)–P(1)–O(20)#2 | 70.9(7) |
| O(20′)–P(1)–O(20) | 70.0(6) | O(20′)#2–P(1)–O(20) | 110.0(7) |
| O(19)#2–P(1)–O(20) | 70.9(7) | O(19)–P(1)–O(20) | 109.1(7) |
| O(20)#2–P(1)–O(20) | 180.0(8) | O(20′)–P(1)–O(19′) | 108.7(6) |
| O(20′)#2–P(1)–O(19′) | 71.3(6) | O(19)#2–P(1)–O(19′) | 108.8(6) |
| O(19)–P(1)–O(19′) | 71.2(6) | O(20)#2–P(1)–O(19′) | 106.8(6) |
| O(20)–P(1)–O(19′) | 73.2(6) | O(20′)–P(1)–O(19′)#2 | 71.3(6) |
| O(20′)#2–P(1)–O(19′)#2 | 108.7(6) | O(19)#2–P(1)–O(19′)#2 | 71.2(6) |
| O(19)–P(1)–O(19′)#2 | 108.8(6) | O(20)#2–P(1)–O(19′)#2 | 73.2(6) |
| O(2A)#1–Ba(1)–O(2A) | 74.7(5) | O(2A)#1–Ba(1)–O(3A)#1 | 139.7(3) |
| O(2A)–Ba(1)–O(3A)#1 | 114.5(3) | O(2A)#1–Ba(1)–O(3A) | 114.5(3) |
| O(2A)–Ba(1)–O(3A) | 139.7(3) | O(3A)#1–Ba(1)–O(3A) | 84.4(4) |
| O(2A)#1–Ba(1)–O(1A) | 78.0(3) | O(2A)–Ba(1)–O(1A) | 137.0(3) |
| O(3A)#1–Ba(1)–O(1A) | 82.1(3) | O(2A)#1–Ba(1)–O(1A)#1 | 137.0(3) |
| O(2A)–Ba(1)–O(1A)#1 | 78.0(3) | O(3A)#1–Ba(1)–O(1A)#1 | 82.1(3) |
| O(3A)–Ba(1)–O(1A)#1 | 69.4(3) | O(1A)–Ba(1)–O(1A)#1 | 141.5(4) |
| O(2A)#1–Ba(1)–O(2)#1 | 69.9(3) | O(2A)#1–Ba(1)–O(2)#1 | 67.2(3) |
| O(3A)#1–Ba(1)–O(2)#1 | 150.4(3) | O(3A)–Ba(1)–O(2)#1 | 79.2(3) |
| O(1A)–Ba(1)–O(2)#1 | 131.3(3) | O(1A)#1–Ba(1)–O(2)#1 | 69.1(3) |
| O(2A)–Ba(1)–O(2) | 67.2(3) | O(2A)–Ba(1)–O(2) | 69.9(3) |
| O(3A)#1–Ba(1)–O(2) | 79.2(3) | O(3A)–Ba(1)–O(2) | 150.4(3) |
| O(1A)–Ba(1)–O(2) | 69.1(3) | O(1A)#1–Ba(1)–O(2) | 131.3(3) |
| O(2A)#1–Ba(1)–O(2) | 125.2(4) | Mo(2)–O(2)–Ba(1) | 165.5(5) |

# $1-x-1, y, -z+3/2$; # $2-x-3, -y+1/2, -z+1$; # $3-x-1, -y, -z+2$.



were placed in calculated positions. The final electron density difference map showed maxima and minima ranging from 1.733 to $-1.212\,e\,Å^{-3}$.

## 3. Results and discussion

### 3.1. *X-ray structure*

The molecular unit of the title compound (figure 1) consists of one anion $[PMo_{12}O_{40}]^{3-}$, one $[Ba(DMF)_6]^{2+}$ complex ion and one unprotoned dma molecule. Crystal structural analysis indicates the polyoxoanion retains the well-known $\alpha$-Keggin-type structure but to some extent it is distorted. As in other Keggin-type structures [16], the $[\alpha\text{-}PMo_{12}O_{40}]^{5-}$ anion is formed from 12 $MoO_6$ octahedra and 1 $PO_4$ tetrahedron. The oxygen atoms in the polyoxoanion can be divided into three groups according to the number of atoms that the oxygen atoms are coordinated to: (1) there are 12 $O_d$ atoms ($O_d$ = terminal oxygen) and the relative Mo–O distances vary in the range of 1.638(8)–1.658(7) Å with the mean value 1.645 Å; (2) there are 24 $O_{b(c)}$ atoms ($O_b$ = bridged oxygen sharing a corner, $O_c$ = bridged oxygen sharing an edge) and the corresponding Mo–O distances vary in the range of 1.839(9)–2.437(12) Å with the mean value 1.934 Å; (3) there are 4 $O_a$ atoms ($O_a$ = oxygen linking with three Mo and one P) and the relevant Mo–O distances vary in the range of 2.438(12)–2.499(12) Å with the mean value 2.463 Å. The Mo–O distances increase with increasing coordination numbers of oxygen atoms as observed in many structures [17, 18]. The $MoO_6$ octahedra are severely distorted. Meanwhile, it can be also seen that Mo(2)–O(2) distance

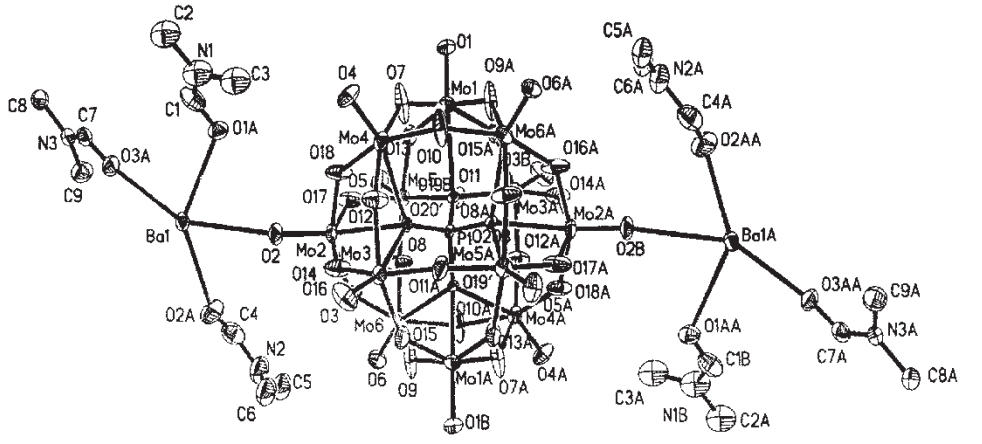


Figure 1. View of the molecular structure unit of the title compound.

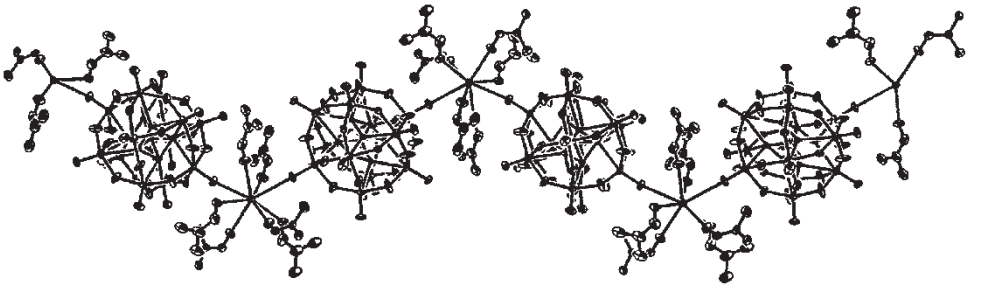

Figure 2. Perspective drawing of the one-dimensional zigzag chain in the title compound.



is 1.658(7) Å, longer than any other Mo–$O_d$ bond lengths. The reason may be that O(2) has coordinated to $Ba^{2+}$ by the terminal oxygen atoms of heteropolyanion through Mo–O–Ba links, confirmed by IR spectra. Because of the different types of organic ions and the different coordination environment, the interactions between the ligands and the polyoxoanions are also different. After DMF molecules are coordinated to $Ba^{2+}$, the interactions between DMF molecules and polyoxoanions will make the Mo–O bonds weaker. From tables 2 and 3, the bond lengths of P–O bonds vary between 1.491(12) and 1.575(12) Å and the bond angles of O–P–O vary between 106.8(6) and 113.1(6)°. Compared with an ideal tetrahedron, the biggest derivation is 4.1°, indicating minor $PO_4$ distortion.

The structure constructed from $[PMo_{12}O_{40}]^{3-}$ and the cations $[Ba(DMF)_6]^{2+}$ exhibits a zig-zag chain with alternating cations and anions through Mo–$O_d$–Ba–$O_d$–Mo links in the crystal (figure 2). The novelty of the composite compound is based on the alternating chains now containing only one cation per anion instead of two [7, 19] (which is observed in other POM–cation chains). The asymmetric units of the compound consist of one $Ba^{2+}$ complex ion and one anion of $[PMo_{12}O_{40}]^{3-}$ linked to a terminal oxygen atom. The coordination environment of $Ba^{2+}$ ion is depicted in figure 3. It can be easily seen from figure 3 that $Ba^{2+}$ is eight-coordinate with a distorted square antiprismatic environment with eight oxygen atoms (six from DMF molecules

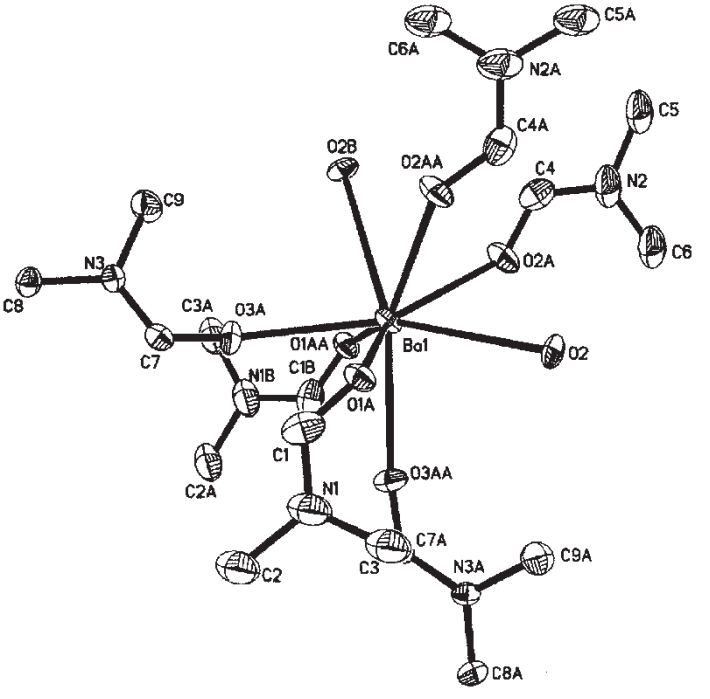


Figure 3. The coordination environment diagram of $Ba^{2+}$ ion.



and the remaining two from adjacent polyanions). In the corresponding polyhedron around $Ba^{2+}$ ion, O(2), O(2A), O(1AA), O(3AA) and O(1A), O(3A), O(2B), O(2AA) lie on two different planes; the average plane derivations are both 0.1275 Å. The Ba–O bond lengths vary in the range of 2.664(10)–3.080(7) Å with mean values of $Ba–O_{(DMF)}$ and $Ba–O_d$ of 2.537 and 3.080 Å, respectively. The $Ba–O_d$ bonds are longer than $Ba–O_{(DMF)}$ bonds, from stronger donating of DMF molecules than $[PMo_{12}O_{40}]^{3-}$. The bond angle for O(2)#1–Ba(1)–O(2) is 125.2(4)°, such that the one-dimensional chain-like structure in the title compound is not straight but zigzag. It is seen from crystal packing of the title compound along the b-axis (figure 4) that the tightest accumulation is realized between chains, in agreement with the demand of the smallest interaction among molecules in the molecular structure. The structure of the title compound is a useful motif for the design of functional molecular assemblies.

### 3.2. *IR and UV spectra*

IR spectra of the complex exhibit four characteristic asymmetric vibrations resulting from heteropolyanions with Keggin structure, namely, $\nu_{as}(Mo{=}O_d)$, $\nu_{as}(Mo–O_b)$, $\nu_{as}(Mo–O_c)$ and $\nu_{as}(P–O_a)$. To compare the IR spectra of the title compound with those of $\alpha$-$H_3PMo_{12}O_{40}\cdot nH_2O$ [19], the vibrational bands of $Mo{=}O_d$, $Mo–O_c$ and $P–O_a$ exhibit red shifts from 975, 810 and 1067 $cm^{-1}$ to 963, 801 and 1062 $cm^{-1}$, respectively, while the vibrational bands of $Mo–O_b$ exhibit blue shifts from 870 to 879 $cm^{-1}$. These results indicate that the polyanion in the compound retains the basic Keggin

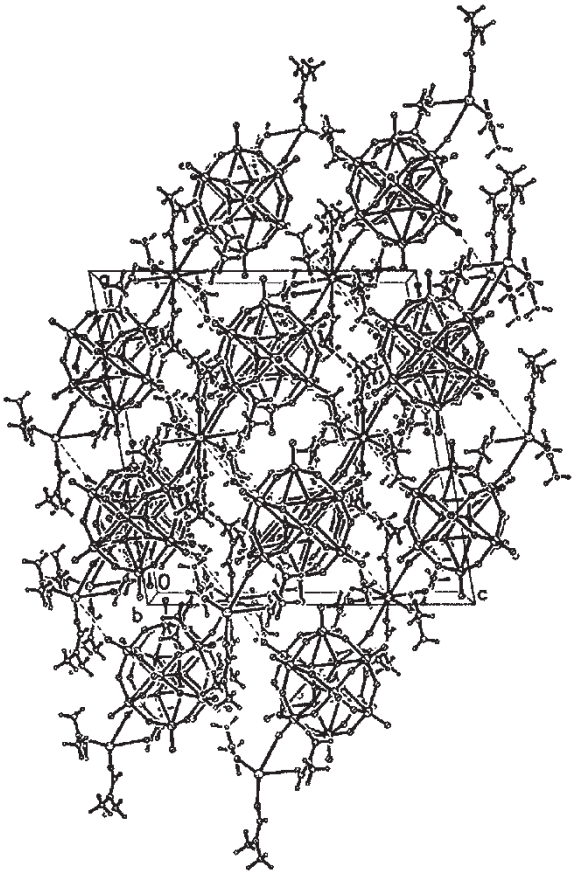


Figure 4. Crystal packing of the title compound along the b-axis.



structure, but is distorted due to the effects of coordination. This is in agreement with the single-crystal X-ray diffraction studies. In addition, there are two characteristic asymmetric vibrations resulting from coordination of DMF molecules, $\nu_{as}$(C=O) and $\nu_{as}$(N–C). Upon comparison of the IR spectra of the compound with those of free DMF, the $\nu_{as}$(C=O) is lower by 23 $cm^{-1}$ (from 1678 to 1655 $cm^{-1}$) confirming that the DMF molecules coordinated to $Ba^{2+}$ ions by the oxygen atoms. The $\nu_{as}$(N–C) frequencies in the compound rise slightly by 2–10 $cm^{-1}$. This can be explained by decreased charge density over the oxygen and carbon centers due to the O atoms of the C=O bonds being coordinated to $Ba^{2+}$, leading to an increase in the electron-donating effect of the methyl groups through N atoms. The IR spectroscopic studies show that there are strong interactions between the polyanions and the organic–metal groups in the solid state.

The UV spectra measured in aqueous solution are similar to that of $\alpha$-$H_3PMo_{12}O_{40} \cdot nH_2O$ in the same solution. According to the literature [20], the absorption peak at approximate 205 nm can be assigned to the $O_d \rightarrow Mo$ charge-transfer bands. This suggests that although the compound exists in polymeric form in the solid state, the polymeric chains are entirely dissociated in dilute solution.

### 3.3. *Thermogravimetric analysis*

The TG curve shows three stages of weight loss. During the first process between 100 and 180°C, the weight loss is 8.67% corresponding to the loss of one dma molecule and 2.5 DMF molecules. There are two endothermal peaks, appearing at 128.3 and 177.4°C in the DTA curve. The second weight loss of 10.08% between 200 and 300°C is ascribed to the release of one structural $H_2O$ and 3.5 DMF. There is an endothermal peak at 265.1°C. The third process starting from 300°C is sublimation of $P_2O_5$. There are three exothermal peaks at 306.7°C (very strong), 383.3 and 461.3°C (weak), and one endothermal peak at 350.1°C in the curve. The exothermal peaks at 306.7 and 383.3°C in the DTA curve indicates that the organic compounds are oxidized. Another exothermal peak indicates that the framework of the title anion decomposes. The title compound is more stable than $\alpha$-$H_3PMo_{12}O_{40} \cdot nH_2O$ [21], than from TG.

### 3.4. *ESR spectra*

To study the ESR, polycrystalline powder was placed into a slim glass tube. The compound is strongly photosensitive towards irradiation with sunlight. Light yellow-green dried powders of the compound turned a deeper color under irradiation with sunlight, resulting in charge-transfer by oxidation of the DMF moieties and reduction of the $[PMo_{12}O_{40}]^{3-}$ groups. ESR spectra of powders of the compound after exposure to sunshine are typical of molybdenum(V) [22, 23] (as shown in figure 5). At 110 K, $g = 1.95$ for the title compound in agreement with the value reported in the literature [24]. The occurrence of the Mo(V) signal ($g = 1.95$) indicates the title compound has formed mixed valence heteropoly blue compound with unshared electrons located in $MoO_6$ octahedra, which results from the electron transfer between organic substrates and the heteropolyanions under irradiation by reduction of the heteropolyanions and oxidation of organic units. According to the literature, the charge transfer may occur through hydrogen bonds [25], but crystal data show that there are no hydrogen

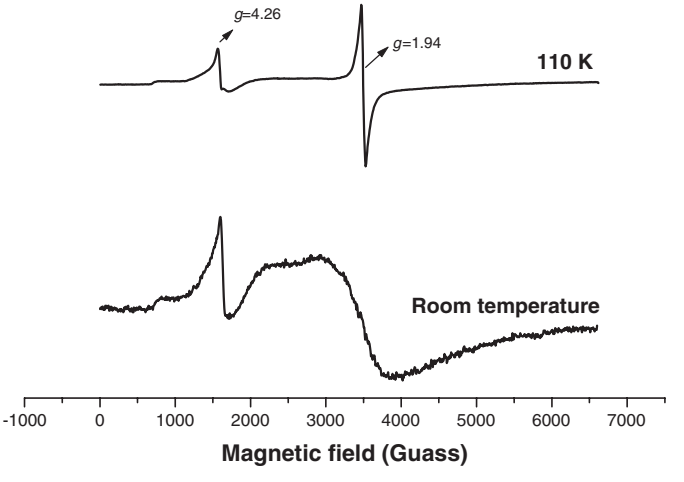


Figure 5. The ESR spectrum of powder of the title compound at 110 K and room temperature.

bonds in the title compound. It is predicted that electronic interactions between the organic substrates and polyoxometalate may result from both secondary Coulombic and induced-dipole effects [26]. Observation of an intense, relatively narrow ESR signal at 3576 G for the title compound at 110 K indicates that intramolecular electron transfer is relatively slow on the ESR timescale, and that the electron is delocalized. Studies on the complete mechanism are currently underway. The other strong line with $g = 4.26$ is ascribed to the absorption band of capillary glass tube. Compared with that at 110 K, spectral width at room temperature is broader because the spin-lattice relaxation time at room temperature is shorter than at 110 K.

### 3.5. *Voltammetric behavior*

Table 4 summarizes the cathodic and anionic peak potentials, the half-wave potentials $E_{1/2}$, as well as the peak potential separation for $\alpha$-$H_3PMo_{12}O_{40} \cdot nH_2O$ and the title compound (in a mixture of 50% 1,4-dioxane and 50% $H_2O$ containing 0.5 mol $L^{-1}$ $H_2SO_4$ as supporting electrolyte, sensitivity 10 μA, $\nu = 50$ mV $s^{-1}$, SCE as the reference electrode). For the phosphomolybdate it is difficult to obtain well-defined redox waves in cyclic voltammetry in aqueous electrolytes due to the ease of hydrolysis of $[PMo_{12}O_{40}]^{3-}$. However, it can be stabilized by addition of comparatively large amounts of organic/aqueous solvent mixtures (50% 1,4-dioxane and 50% redistilled $H_2O$) containing 0.5 mol $L^{-1}$ $H_2SO_4$ as the supporting electrolyte, in which the phosphomolybdate anion exhibits a kinetically stable and reproducible cyclic voltammetric pattern. $\alpha$-$H_3PMo_{12}O_{40} \cdot nH_2O$ as well as the title compound undergoes five two-electron reversible reduction processes. The reversibility criterion used was $\Delta E_p = E_{ap} - E_{cp} = 59/n$ mV ($n$ = number of electrons).

To highlight the influence of pH value on the peak potentials in the cyclic voltammograms for the title compound, the following experiments were carried out in the same above-mentioned media in the wide pH region, where the pH value was adjusted by 1 mol $L^{-1}$ NaOH aqueous solution. The cyclic voltammograms (as shown in figure 6) in the pH range of 0.32–4.00 have five two-electron charge-transfer processes and the redox potentials decrease with increasing pH. Reduction of $[PMo_{12}O_{40}]^{3-}$ immobilized is accompanied by the evolution of protons from solution to the surface of the electrode

Table 4. Cathodic peak potentials ($E_{cp}$) and anodic ($E_{ap}$) and the peak potentials separation for $\alpha$-$H_3PMo_{12}O_{40} \cdot nH_2O$ and the title compound (in the mixture of 50% 1,4-dioxane and 50% $H_2O$ containing 0.5 mol $L^{-1}$ $H_2SO_4$ as the supporting electrolyte, sensitivity 10 μA, scan rate: 50 mV $s^{-1}$ SCE as the reference electrode).

| Compound | $E_{cp}$ (V) | $E_{ap}$ (V) | $\Delta E_p$ (mV) | $E_{1/2}$ (V) |
|---|---|---|---|---|
| $\alpha$-$H_3PMo_{12}O_{40} \cdot nH_2O$ | 0.308 | 0.339 | 31 | 0.324 |
| | 0.179 | 0.208 | 29 | 0.194 |
| | −0.052 | −0.022 | 30 | −0.037 |
| | −0.201 | −0.17 | 31 | −0.186 |
| | −0.282 | −0.244 | 38 | −0.263 |
| $\{H[Ba(DMF)_6(PMo_{12}O_{40})] \cdot (dma)\}n$ | 0.333 | 0.368 | 35 | −0.350 |
| | 0.211 | 0.246 | 35 | 0.229 |
| | −0.025 | 0.013 | 38 | −0.006 |
| | −0.164 | −0.129 | 35 | −0.147 |
| | −0.300 | −0.261 | 39 | 0.2811 |

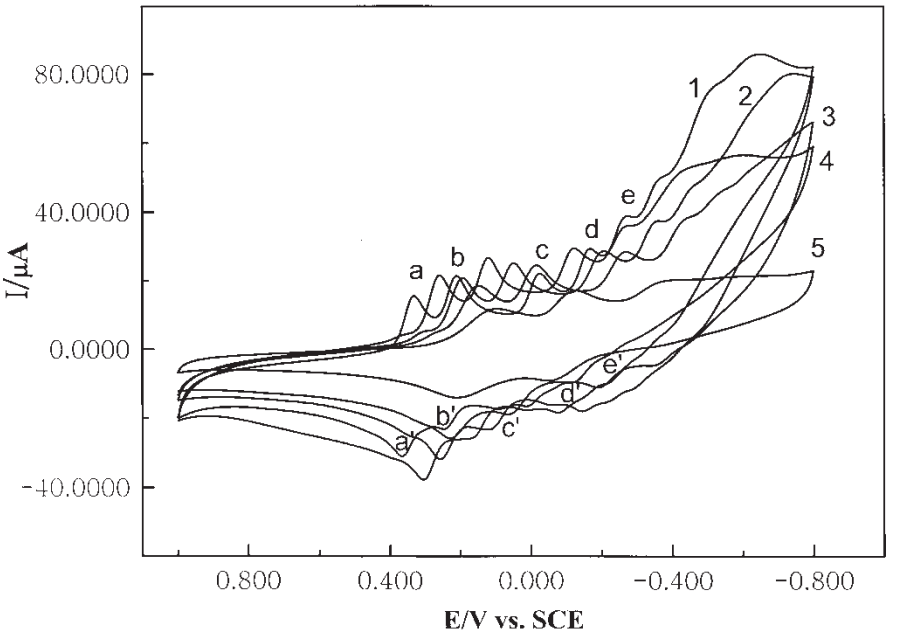


Figure 6. Cyclic voltammograms of $\{H[Ba(DMF)_6(PMo_{12}O_{40})]\cdot(dma)\}_n$ ($1\,mmol\,L^{-1}$) in the mixture of 50% 1,4-dioxane and 50% $H_2O$ containing $0.5\,mol\,L^{-1}$ $H_2SO_4$; scan rate: $50\,mV\,s^{-1}$. The pH value was adjusted with $1\,mol\,L^{-1}$ NaOH aqueous solution. Curves 1: pH = 1.00, 2: pH = 2.00, 3: pH = 3.00, 4: pH = 0.32, 5: pH = 4.00.

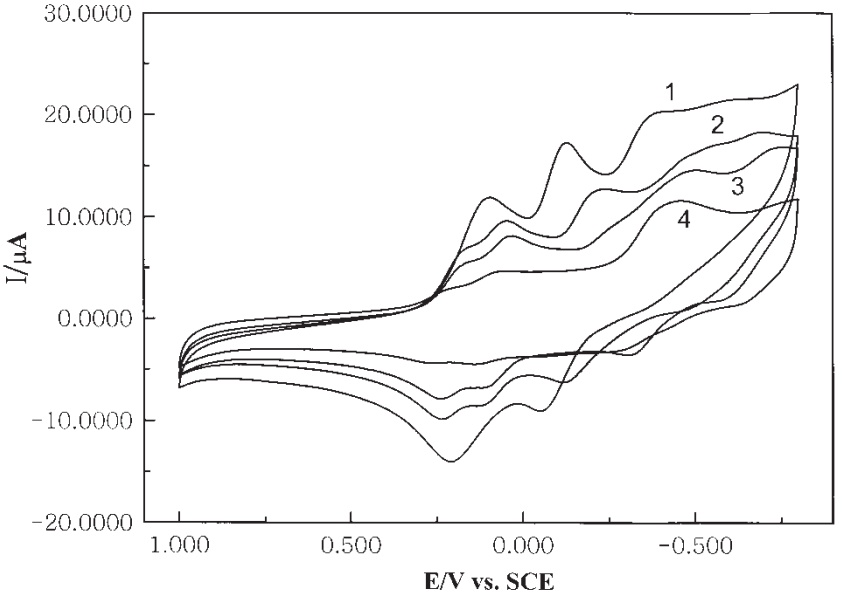


Figure 7. Cyclic voltammograms of $\{H[Ba(DMF)_6(PMo_{12}O_{40})]\cdot(dma)\}_n$ ($1\,mmol\,L^{-1}$) in the mixture of 50% 1,4-dioxane and 50% $H_2O$ containing $0.5\,mol\,L^{-1}$ $H_2SO_4$; scan rate: $50\,mV\,s^{-1}$. The pH value was adjusted with $1\,mol\,L^{-1}$ NaOH aqueous solution. Curves 1: pH = 4.00, 2: pH = 5.00, 3: pH = 6.00, 4: pH = 7.00.

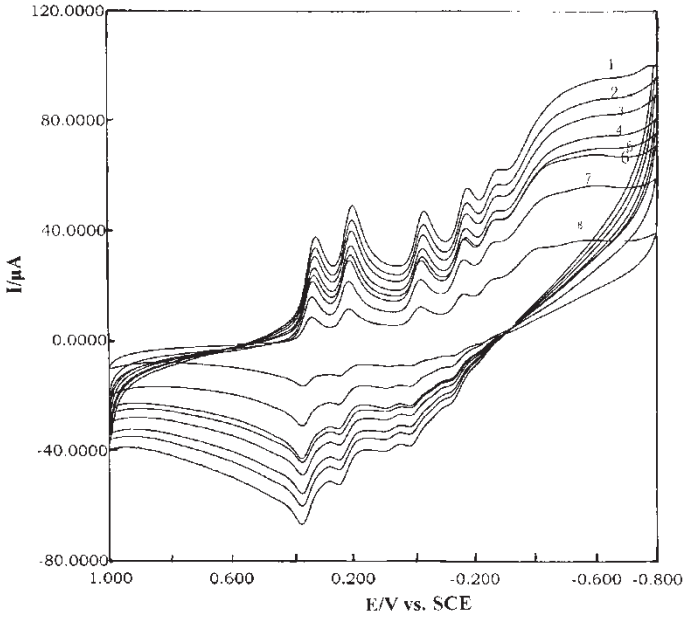


Figure 8. Cyclic voltammograms of $\{H[Ba(DMF)_6(PMo_{12}O_{40})]\cdot(dma)\}_n$ (1 mmol $L^{-1}$) in the mixture of 50% 1,4-dioxane and 50% $H_2O$ containing 0.5 mol $L^{-1}$ $H_2SO_4$; Curves 1: $\nu = 200\,mV\,s^{-1}$, 2: $\nu = 70\,mV\,s^{-1}$, 3: $\nu = 150\,mV\,s^{-1}$, 4: $\nu = 120\,mV\,s^{-1}$, 5: $\nu = 100\,mV\,s^{-1}$, 6: $\nu = 80\,mV\,s^{-1}$, 7: $\nu = 50\,mV\,s^{-1}$, 8: $\nu = 20\,mV\,s^{-1}$.

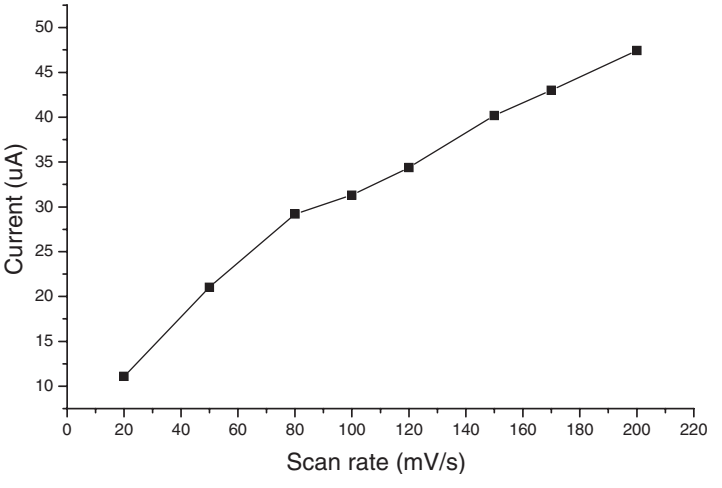


Figure 9. Dependence of anodic peak current on scan rates.

to maintain charge neutrality. As the pH value increases, negative shift of the reduction peaks potential can be elucidated by the Nernst equation [27]. However, all the peak potentials in the pH value from 4.00 to 7.00 (figure 7) are in agreement with those in the pH value of 4.00. At pH = 4.00, as the processes of a–a′ and d–d′ the oxidation peaks disappear whereas for the b–b′ and c–c′ processes, the oxidation peaks become weaker than before. The redox processes are gradually becoming irreversible with

increasing pH, which may be due to hydrogen evolution or framework change of the polyanion. On the contrary, with increasing solution pH, the oxidation peaks are turning stronger step by step, indicating degeneration of the increasing solution alkalinity. From the above analysis, the solution pH value in the low pH value region has a more intense influence on the peak potentials.

Cyclic voltammograms of the title compound at different scan rates (figure 8) indicate that the peak currents increase with increasing scan rates, but the peak potentials hardly change with increasing scan rates. Plots of peak current *versus* scan rate are shown in figure 9. When the scan rate was varied from 20 to 200 mV $s^{-1}$, the cathodic peak currents were almost the same as the corresponding anodic peak currents. At scan rates lower than 80 mV $s^{-1}$, the anodic currents were proportional to the scan rate, suggesting that the electron-transfer is a reversible surface process [28]. However, at scan rates higher than 80 mV $s^{-1}$, the anodic currents were proportional to the square root of the scan rates, indicating that the redox process is diffusion-controlled.



## Supplementary material

Crystallographic data have been deposited with the Cambridge Crystallographic Data Center with the deposited numbers CCDC Number 236441. Copies of this information may be obtained free of charge free from The Director, CCDC, 12 Union Road, Cambridge, CB2 1EZ, UK (Fax: +44-1223-336033; e-mail: deposit@ccdc.cam.ac.uk).

## Acknowledgements

This work was supported by the Natural Science Foundation of Henan Province and the Department of Education Foundation of Henan Province.

## References

[1] Z.R. Liu, L. Wang, E.B. Wang, L. Xu, Y. Xing, Y.H. Lin, H.Q. Jia. *Chem. J. Chin. Univ.*, **20**, 1842 (1999).
[2] Y.H. Wang, C.W. Hu, E.B. Wang, N.H. Hu, H.Q. Jia, Y. Xing. *Chem. J. Chin. Univ.*, **22**, 362 (2001).
[3] E. Coronado, C.J. Gomez-Garcia. *Chem Rev.*, **98**, 273 (1998).
[4] C.J. Gomez-Gareia, C. Gimenea-Saiz, S. Trik, E. Coronado, P. Le Magueres, L. Ouahab, L. Ducasse, C. Sourisseau, P. Delhaes. *Inorg. Chem.*, **34**, 4139 (1995).
[5] E. Coronado, J.R. Galan-Macaros, C. Gimenez-Saiz, C.J. Gómez-García, C. Rovira, J. Tarrés, S. Triki, J. Veciana. *J. Mater. Chem.*, **8**, 313 (1998).
[6] P. Le Magneres, L. Ouahab, S. Golben, D. Grandjean, O. Pena, J.-C. Jegaden, C.J. Gómez-García, P. Delhaes. *Inorg. Chem.*, **33**, 5180 (1994).
[7] J.P. Wang, Q. Wu, J.Y. Niu. *Science in China (series B)*, **32**, 210 (2002).
[8] J.P. Wang, J.W. Zhao, J.Y. Niu, D.J. Guo, D.B. Dang, *Science in China (series B)*, **33**, 397 (2003).
[9] J.Y. Niu, J.P. Wang, W. Chen, C.H.L. Kennard, K.A. Byriel. *J. Coord. Chem.*, **53**, 13 (2001).
[10] J.P. Wang, D.J. Guo, J.Y. Niu. *Chin. J. Appl. Chem.*, **9**, 852 (2002).
[11] J.Y. Niu, J.P. Wang, Y. Bai, D.B. Dang, L. Yu. *Chem. Res.*, **11**, 14 (2000).
[12] B. Xie, J.S. Li, Z.N. Men. *Acta. Chimica. Sinica.*, **56**, 263 (1998).
[13] R.D. Claude, F. Michael, F. Raymonde, T. Rene. *Inorg. Chem.*, **22**, 207 (1983).
[14] G.M. Sheldrick. *SHELXS 97, Program for Structure Refinement*, University of Güttingen, Germany (1997).
[15] G.M. Sheldrick. *SADABS, A Program for Absorption Correction with Braker SMART System*, University of Göttingen, Germany (1996).

[16] M.T. Pope. *Heteropoly and Isopoly Oxometalates*, Springer-Verlag, New York (1983).
[17] R. Strandberg. *Acta Chem. Scand. A*, **29**, 350 (1975).
[18] Y.K. Shan, Z.X. Liu, Z.S. Jin, G.C. Wei. *J. Struct. Chem.*, **11**, 92 (1992).
[19] J.Y. Niu, Q. Wu, J.P. Wang. *J. Chem. Soc. Dalton*, **12**, 2512 (2002).
[20] G.Y. Fu, E.B. Wang, J.F. Liu, R.L. Zheng. *Acta. Chimica. Sinica*, **43**, 949 (1985).
[21] J.Y. Niu, J.P. Wang. *Introduction of Heteropoly Compound*, Henan University Pree, Kaifeng, 343 (2000).
[22] C. Sanshez, J. Livage, J.P. Laybat, M. Fournier, Y. Jeannin. *J. Am. Chem. Soc.*, **1040**, 3194 (1982).
[23] J.N. Barrow, M.T. Pope. *Adv. Chem. Ser.*, **226**, 403 (1990).
[24] M.T. Pope. Mixed-valence compounds. In *Heteropoly Blues*, Reidel, Oxford (1979).
[25] J.Y. Niu, X.Z. You, C.Y. Duan, H.K. Fun, Z.Y. Zhou. *Inorg. Chem.*, **35**, 4211 (1996).
[26] M.M. Williamson, D.A. Bouchardm, C.L. Hill. *Inorg. Chem.*, **26**, 1436 (1987).
[27] J. Wang. *Analytical Electrochemistry*, VCH, New York (1994).
[28] R.W. Murray. In *Electroanalytical Chemistry*, A.J. Bard (Ed.), Vol. 13, Marcel Dekker, New York, p. 191 (1984).